Examining diel patterns of soil and xylem moisture using electrical resistivity imaging

Rachel Mares [a], Holly R. Barnard [b], Deqiang Mao [c], André Revil [d], Kamini Singha [a,e,*]

[a] Colorado School of Mines, Hydrologic Science and Engineering Program, Golden 80401, CO, USA
[b] University of Colorado at Boulder, Institute of Arctic and Alpine Research, Department of Geography, Boulder 80309, CO, USA
[c] Colorado School of Mines, Department of Geophysics, Golden 80401, CO, USA
[d] ISTerre, CNRS, UMR CNRS 5275, Université de Savoie Monte-Blanc, 73376 cedex, Le Bourget du Lac, France
[e] Colorado School of Mines, Department of Geology and Geological Engineering, Golden 80401, CO, USA

ARTICLE INFO

SUMMARY

The feedbacks among forest transpiration, soil moisture, and subsurface flowpaths are poorly understood. We investigate how soil moisture is affected by daily transpiration using time-lapse electrical resistivity imaging (ERI) on a highly instrumented ponderosa pine and the surrounding soil throughout the growing season. By comparing sap flow measurements to the ERI data, we find that periods of high sap flow within the diel cycle are aligned with decreases in ground electrical conductivity and soil moisture due to drying of the soil during moisture uptake. As sap flow decreases during the night, the ground conductivity increases as the soil moisture is replenished. The mean and variance of the ground conductivity decreases into the summer dry season, indicating drier soil and smaller diel fluctuations in soil moisture as the summer progresses. Sap flow did not significantly decrease through the summer suggesting use of a water source deeper than 60 cm to maintain transpiration during times of shallow soil moisture depletion. ERI captured spatiotemporal variability of soil moisture on daily and seasonal timescales. ERI data on the tree showed a diel cycle of conductivity, interpreted as changes in water content due to transpiration, but changes in sap flow throughout the season could not be interpreted from ERI inversions alone due to daily temperature changes.

1. Introduction

Ecological controls on hydrologic pathways and storage in forested catchments are often most pronounced during low-flow or baseflow conditions, which typically coincide with the growing season in temperate environments. At these times, evapotranspiration (ET) can comprise greater than 50% of the water that exits the catchment (Hewlett, 1982) and regulates catchment storage. Despite significant correlations between transpiration and diel (24-h) streamflow in catchments of varying sizes and locations (Reigner, 1966; Bond et al., 2002; Boronina et al., 2005; Butler et al., 2007; Barnard et al., 2010; Graham et al., 2013), how the transpiration signal is propagated throughout the subsurface is dependent on complex, connected mechanisms, and remains poorly understood (e.g., Richards and Caldwell, 1987; Burgess et al., 2000; Bleby et al., 2010). For example, stable isotope studies have indicated that water extracted by forests differs from water generating baseflow in some streams, suggesting a complicated system of subsurface connections (Dawson and Ehleringer, 1991; Brooks et al., 2010).

Diel fluctuations in soil moisture are common in vegetated areas where water content declines during the day when transpiration extracts water from the subsurface and may partially recover throughout the night (Barnard et al., 2010; Moore et al., 2011). Two mechanisms have been proposed to explain the recovery of soil moisture during the night: diffusion recharge and hydraulic redistribution. For the first mechanism, soil moisture may be transferred within the soil matrix simply by diffusion from wetter areas to drier areas; however, this process is very slow and its impact is likely minimal (Richards and Caldwell, 1987; Domec et al., 2010). For hydraulic redistribution, roots passively move soil moisture from plentiful areas to water-depleted areas in the lateral or vertical direction due to diurnal changes in the water potential gradient between the root and the soil matrix (Caldwell and Richards, 1989; Dawson, 1993; Burgess et al., 1998). During transpiration, the water potential within the plant declines below that

of the soil resulting in a net flux of water into the roots. When transpiration ceases, the water potential in the roots can rise higher than the potential in the soil, allowing water to move back into the soil matrix. Estimates of the average amount of water moved by hydraulic redistribution range two orders of magnitude (0.04–3.2 mm/d) across species and ecosystems (e.g., Neumann and Cardon, 2012). Although several studies have now documented hydraulic redistribution, understanding the complexities of root distributions and their role in hydrologic connectivity in the subsurface remains a pressing concern in hydrology (Good et al., 2015; Evaristo et al., 2015).

Quantifying vegetation–subsurface connections is difficult due to complexities in measuring the dynamic and heterogeneous nature of plant root distributions, water uptake patterns, transpiration, and soil moisture inputs, all of which are difficult to capture with standard point measurements. Soil moisture is commonly measured using techniques such as time-domain reflectometry (TDR), gravimetric (mass) methods, direct-push based sensor probes, and neutron probes (e.g., Dobriyal et al., 2012). One common limitation of many soil moisture measurement techniques is the limited spatial coverage in heterogeneous soil plots; additionally most measurement techniques exploring root systems and soil moisture are disruptive to the soil matrix (Maeght et al., 2013). Not only are physical soil characteristics heterogeneous in forest environments, but so is the effect of transpiration and tree interception on the spatial distribution of water content, which is key to characterizing water movement within vadose zone. In trees, sap flow sensors, which use heat as a tracer for water movement, are commonly used for monitoring and quantifying transpiration (e.g., Granier, 1987; Burgess et al., 2001). Sap flux is a point measurement that is typically scaled up based on an assumed uniform radial sapwood distribution, making it susceptible to errors due to asymmetry of the sapwood thickness. Such asymmetry can be caused by branching, slope aspect, and reaction wood formation and can result in over- or under-estimation of total tree transpiration when using a limited number sampling points (Vertessy et al., 1997). Additionally, if diurnal and seasonal variation in sapflux rates between the inner and outer xylem are not accounted for, total daily transpiration can be overestimated by up to 40% (Ford et al., 2004; Fiora and Cescatti, 2006).

Geophysical methods can be used to overcome some of the limitations of point measurements through minimally invasive, spatially exhaustive, 3D monitoring without sacrificing temporal resolution. For example, electrical resistivity imaging (ERI) has been a well-established method to image changes in soil moisture for several decades (e.g., Daily et al., 1992; Zhou et al., 2001; Samouëlian et al., 2005; Chambers et al., 2014). Bouyoucos and Mick (1940) buried porous plaster-of-Paris blocks that were embedded with electrodes into soil plots and saw changes in conductivity as the soil moisture content ranged from field capacity to wilting point. More recently, ERI has been successfully used to monitor spatial and temporal soil moisture distributions in heterogeneous areas such as naturally vegetated hillslopes (e.g., Brunet et al., 2010), across vegetation boundaries (e.g., Jayawickreme et al., 2010), and most commonly, in agricultural systems (e.g., Hagrey and Michaelsen, 2002; Schwartz et al., 2008; Beff et al., 2013; Garré et al., 2013). Some agricultural applications of ERI have looked to help optimize soil water reserves and irrigation practices by imaging areas of high infiltration and drainage (e.g., Banton et al., 1997; Michot et al., 2003), or to explore water vs. nutrient limitations in cropped fields when used in conjunction with carbon isotopic data (Hussain et al., 2015). ERI has been used to explore root water uptake in a variety of settings, including in sand dunes during rainfall (Fan et al., 2015), in agricultural field sites under irrigated treatments (e.g., Srayeddin and Doussan, 2009; Cassiani et al., 2015), as well as at the large-lysimeter scale (e.g., Garré

et al., 2011); diel cycling of water content is something noted in some of these data sets (e.g., Werban et al., 2008). These data may also be useful for understanding soil moisture persistence (e.g., Ghannam et al., 2016) over broad scales. Although there are uncertainties associated with the reconstructed bulk electrical conductivity maps made from resistance data, ERI provides better spatial resolution than dense arrays of point measurements such as TDR (Schwartz et al., 2008; Nijland et al., 2010); however, the relation between moisture content and electrical conductivity is spatially variable and dependent on multiple variables, making estimates of moisture content directly difficult (e.g., Friedman, 2005; Day-Lewis et al., 2005; Garré et al., 2013).

Here, we explore the connection between soil moisture and tree transpiration coupling traditional point-scale measurements with ERI to monitor spatially exhaustive moisture content changes within the soil and tree throughout a growing season. ERI has previously been applied to a few studies in forest ecology. In an early study, Tattar et al. (1972) used resistance measurements to determine the stage of deterioration of decaying or discolored wood. ERI has also been used to study living trees; for example, Hagrey (2006) found an inverse relation between ERI and moisture content measured from tree cores. ERI has successfully imaged cavities and fungus within tree trunks (Skutt et al., 1972; Nicolotti et al., 2003; Hagrey, 2006) and delineated sapwood from heartwood (Hagrey, 2006; Bieker and Rust, 2010; Guyot et al., 2013; Wang et al., 2015). The resistivity within trees varies significantly among species, and these results suggest these variations are due to anatomical and physiological differences (Gora and Yanoviak, 2015). While diel fluctuations in tree sap flow have been measured by naturally occurring voltages (Gibert et al., 2006), to the best of our knowledge, no time-lapse ERI studies within trees as coupled to the subsurface have been employed. Here, we aim to (1) evaluate the application of ERI as a minimally invasive method to monitor high-resolution spatial and temporal changes in soil and tree water content during one growing season and into the fall and (2) relate these water content patterns to the seasonal variation in transpiration and explore their feedbacks.

2. Material and methods

We collected a series of data around a single ponderosa pine surrounded by several meters of open space so that potential effects from nearby trees were minimized. The closest neighboring tree is 4 m east of the study tree. The data collected included electrical conductivity of the soil and tree, soil moisture content, sap flow, and soil and bole temperature.

2.1. Field site description

The study site is located in the Gordon Gulch catchment within the Arapahoe National Forest in the Boulder Creek Critical Zone Observatory (BCCZO) in Boulder, Colorado (Fig. 1). The general goal of the BCCZO is to explore the role of weathering and erosion on the form and function of the shallow subsurface. Gordon Gulch is approximately 2.7 km^2 and ranges from 2446 to 2737 m in elevation within the upper montane climatic zone. Average annual precipitation is 519 mm with the maximum occurring in May, and potential evapotranspiration is ≈500 mm/year. The soils are characterized as typic haplustolls varying in composition with depth. Percent sand by weight ranges from 55% to 65%. Silt ranges from 25% to 50% with higher silt content in the shallow layers (<20 cm depth) and lower contents in deeper layers. Average clay content is approximately 10%. Along the hillslopes, soil depth is approximately 30–50 cm (NRCS Soil Survey, 2015); at our site soil depth is approximately 30–35 cm. The soil profile is underlain by highly
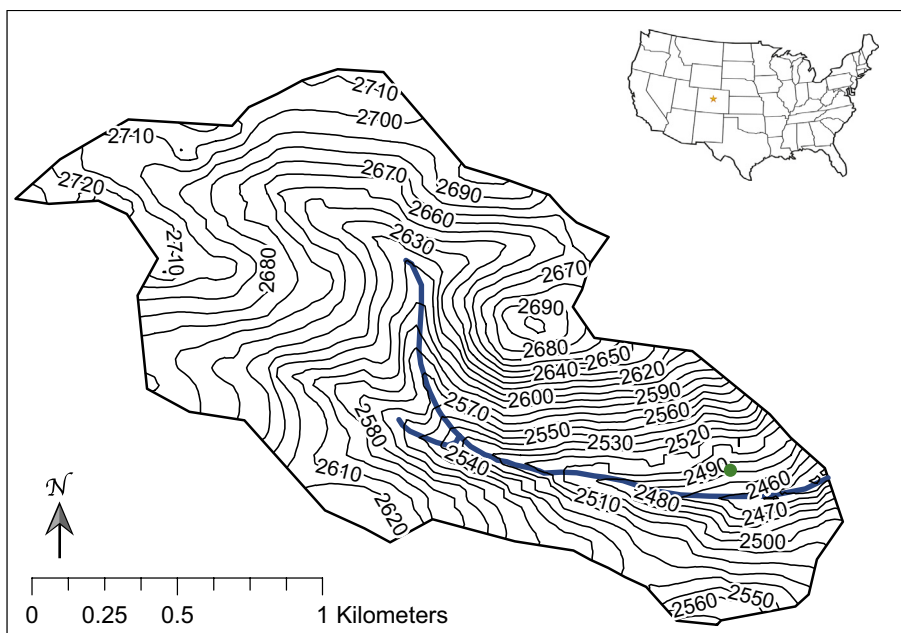
Fig. 1. Map of the study area with Gordon Gulch (blue line), location of the study tree (green dot), and 10 m contours. (For interpretation of the references to color in this figure legend, the reader is referred to the web version of this article.)

weathered rock that extends five to seven meters in depth (Befus et al., 2011). Limited water level data exist within the watershed; no deep wells have been drilled in lower Gordon Gulch, and three deep wells in upper Gordon Gulch show depths to water of approximately 5–11 m below land surface, depending on the time of year (http://criticalzone.org/boulder/).

The catchment contains three distinct types of vegetation cover: (1) aspen (*Populus tremuloides*) groves near the stream, (2) open meadows, and (3) the forested hillslopes. The north-facing hillsides are densely vegetated by lodgepole pine (*Pinus contorta*) and some western Douglas-fir (*Pseudotsuga menziesii*). The south-facing slopes support less densely vegetated areas of ponderosa pines (*Pinus ponderosa*). The ponderosa pine individual used in this study was approximately 15 m tall and approximately 40 cm in diameter at breast height (DBH), and is located on a south-facing slope near the southeast edge of the catchment (40°0′46.289″N, 1 05°27′43.715″W) approximately 100 m north of the Gordon Gulch stream, and was chosen as a representative pine, based on DBH, of those on the south-facing hillslopes of this catchment. The average DBH for trees in the vicinity of the study tree is 30.3 cm (standard deviation = 9.4 cm). The average stand density of ponderosa pine forest in lower Gordon Gulch is approximately 600 trees/ha. This is about equivalent to a 4 m × 4 m spacing among individual trees. Digging up lateral roots is not feasible at this site, but ponderosa pine can have shallow, laterally expanding main roots that extend 10–40 m in open grown conditions (Berndt and Gibbons, 1958; Schenk and Jackson, 2002), and rooting depths of at least 2 m and up to 12 m (Stone and Kalisz, 1991; Ryan et al., 2000).

2.2. Data collection

Time-lapse ERI data were collected on a square plot surrounding the tree to monitor changes in soil moisture (for a review on ERI methods, see Binley and Kemna, 2005). Sixty-three 25 cm long stainless steel electrodes were inserted into the ground approximately 10 cm, forming a 3.5 m by 3.5 m grid around the tree (Fig. 2a). Each row and column contained 8 electrodes spaced 0.5 m apart, with some minimal variability due to difficulties inserting electrodes at the exact distance with surface hetero-

geneities. Due to the location of the tree, one row contained only 7 electrodes. An IRIS Syscal Pro Switch 96 (IRIS Instruments, Orléans, France) coupled with an IRIS switch box was used to collect ERI data. To shorten data collection time to capture the expected diel cycling with high temporal resolution, a dipole–dipole array with up to skip-4 separation in each direction was used. This array provides the advantage of better resolving lateral variations in conductivity than other arrays. Current is injected into two electrodes and the potential difference is measured at up to 10 other pairs of electrodes along 2-D lines simultaneously. Approximately every 30 min, a series of 16 2D surveys were collected, one down each column and across each row of the electrode grid for a total of 240 quadripoles. Data were collected for periods varying from 24 to 48 h approximately every two weeks from May to October in 2014. These time frames were chosen to examine the spatial and temporal changes of soil moisture influenced by tree transpiration on both daily and seasonal time scales. The contact resistance between the electrodes and the soil plot were generally below 20 kΩ (median value = 10 kΩ), which we considered reasonable for the sandy soils. Measurements were stacked for quality assurance/quality control due to time limitations. All measurements were stacked twice; less than 0.5% of the data had a stacking error greater than 2%. Approximately 50 datasets were collected during each 24-h data collection period.

Time-lapse ERI surveys were also performed on the xylem within the bole of the tree, on a radial section of the tree trunk, at each time step to relate the changes in bole conductivity with sap flow measurements. Steel nails (4 mm diameter) were used as electrodes and hammered 2–3 cm into the xylem of the tree. The electrodes were placed one meter above the ground to avoid the effects of axial boundary conditions in the inversion, which become significant when the electrodes are too close to the ground (more details on this are outlined in the section on inversion). The 24 electrodes were spaced 5 cm apart, forming a ring around the 125-cm circumference of the tree and connected to the IRIS switch box (Fig. 2b). A dipole–dipole survey, again with electrode separation up to skip 4, was used for speed; a total of 414 quadripoles were collected. Contact resistance between the electrodes within the tree xylem was approximately 100 kΩ,
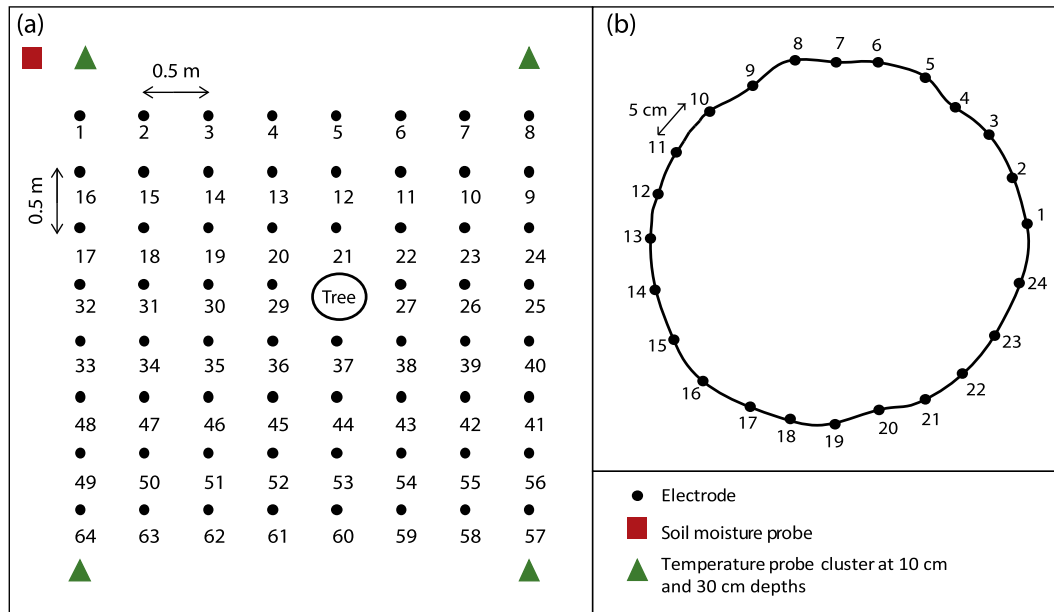
Fig. 2. The electrode grid for ground conductivity surveys (a). Spacing is 0.5 m between each electrode. Temperature probe clusters are placed outside the grid to minimize their effect on conductivity surveys. Electrode configuration for the conductivity surveys on the trunk of the tree (b).

which restricted current from being driven into the tree for parts of the surveys. Approximately 40% of the data were not used due to this issue. Despite this, approximately 200 data points were still collected with reasonable stacking errors (a mean of 1.3%) at each time step; data were again stacked twice. The circumference of the tree was measured using a large plastic hoop and a measuring tape. The hoop was mounted perpendicularly to the tree trunk, surrounding it, and the shortest distance from the hoop to each electrode on the tree was noted. This geometry was used to calculate the angle of each electrode on a circle. Using the angle, the distance from the hoop to the electrode, and simple geometry, the geometry of the tree and coordinates of the electrodes were calculated.

A suite of auxiliary data was also collected at the site. To compare ERI measurements to transpiration, we installed heat-pulse ratio sap flow sensors that we built based on Burgess et al. (2001), which have a sensitivity of ±8% in sapflux (Steppe et al., 2010). Sensors were installed at 1.5 m above the ground surface in eight ponderosa pine trees within 60 m of the study tree. The DBH of the sap flow measurement trees ranged from 19 to 47 cm (average of 33 cm). Sap flow was not measured directly in the study tree to avoid any feedbacks between the sap flow instrumentation (stainless steel probes) and ERI electrodes that both inject current into the tree. While the magnitude of sap flow varied in the eight trees, the highest sapflux velocity was at 11 am for seven of the eight trees (the 8th was at 11:30 am; Fig. 3). Variance in timing of transpiration was minimal, allowing these data to be meaningful proxies to the ERI-instrumented tree. Additionally, at the end of our study period, we collected seven tree cores from around the circumference of the tree to determine the location of heartwood as well as sapwood (water conducting xylem) and heartwood (non-conducting xylem) moisture content. To do so, we sampled the xylem of the study tree and its two nearest neighboring trees using a 5-mm diameter increment borer (n = 4 cores per non-study tree). Each xylem sample was divided into sapwood and heartwood based on wood opacity. Fresh core samples were sealed in plastic straws and stored in a cooler to prevent evaporation. In the lab, samples were removed from straw, weighed and then dried at 70 °C for 48 h, and reweighed to determine moisture content.
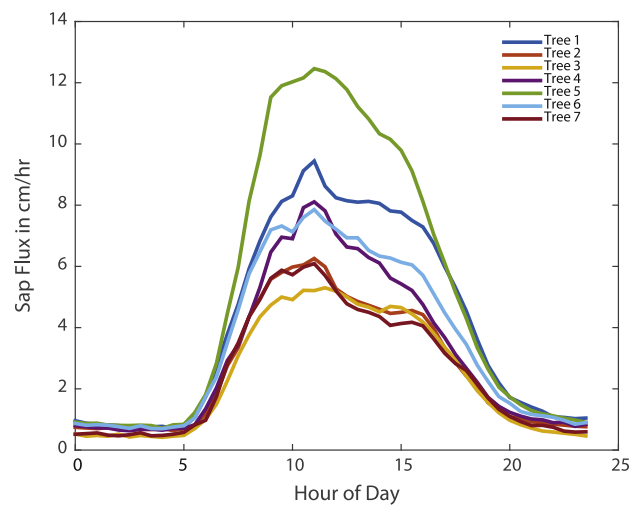
Fig. 3. Average sap flux measurements from instrumented trees for all measurement days from June 3 to November 10, 2014.

Soil volumetric water content was measured at one location 0.5 m outside of the upper left corner of the electrode grid and collected data every 15 min at 10 cm and 20 cm depths with Decagon EC-5 sensors (±3% error in volumetric water content) and a CR1000 data logger (Fig. 2a). Deeper probes could not be installed as the soil on the south-facing slope, which has an average depth of 30–35 cm to saprolite (Hinckley et al., 2014). The porosity of the soil plot was assumed constant in time; therefore, the change in volumetric water content was used as a proxy for the change in soil moisture over time. These data, unfortunately, were not continuous, so we also used water content measurements collected at a site 55 m away, and biased away from tree roots, to look at seasonal changes. These soil moisture measurements were collected every 30 min, continuously for years, at 10 and 30 cm depth using Hydra Probes II from Stevens Water Monitoring Systems, Inc.

Lastly, temperature data were collected for the soil, air, and tree xylem throughout the study period to correct ERI data for changes

in temperature. HOBO Pendant Temperature and Light Loggers (±0.5 °C error in temperature) were placed in the soil at 10 cm and 20 cm depth outside each corner of the electrode grid—two sensors in each quadrant. The temperature within the tree xylem was measured with a CR1000 data logger and three type T (copper-constantan) thermocouples (±1% error in temperature) placed 2–3 cm into the xylem and 12 cm above tree electrodes 1, 9, and 17 (Fig. 2b). Canopy air temperature and relative humidity (collected within the sapflow plot) were used to calculate the vapor pressure deficit (VPD) after Monteith and Unsworth (1990).

2.3. Raw ERI data analysis

The raw apparent conductivity data from the tree and ground were used to examine the general temporal trends prior to inversion. Data with stacking standard deviation values greater than 2.5% and 10% were excluded from the ground and tree datasets, respectively, for exploring the raw data.

2.4. Ground survey inversions

Ground survey inversions of apparent electrical conductivity data were inverted using R2 version 2.7 (Binley and Kemna, 2005), based on a regularized objective function combined with weighted least squares:

$$\psi(\boldsymbol{m}) = (\boldsymbol{W_d}[\boldsymbol{d} - f(\boldsymbol{m})])^2 + \beta(\boldsymbol{W_m}[\boldsymbol{m} - \boldsymbol{m_{ref}}])^2 \qquad (1)$$

where $\boldsymbol{m}$ is the model vector of resistivities (the reciprocal of conductivity), $\boldsymbol{d}$ is the measured resistance data, $\boldsymbol{W_d}$ is the data weighting matrix based on measurement error reported as standard deviation of each repeated measurement, $f(\boldsymbol{m})$ is the forward solution of the resistances operating in the model, $\boldsymbol{W_m}$ is the model weighting matrix based on a second-derivative filter that acts as a smoother, β is the weight that controls the relative significance of the model misfit (first term on the right) and the model roughness (second term on the right), and $\boldsymbol{m_{ref}}$ is the starting model. The time-lapse conductivity inversions from each collection period were performed with a starting model ($\boldsymbol{m_{ref}}$) that was equal to the inversion of the first time-step of each two-day collection period, and a description of the time-lapse inversion can be found in Binley and Kemna (2005). For each time-step, a 2.5D inversion was performed on each of the 16 ground ERI surveys. 2.5D inversion allows for reconstruction of a 2D plane from data while simulating the source in 3D; details can be found in Dey and Morrison (1979). No data were filtered in advance of the inversions; data were weighted in $\boldsymbol{W_d}$ above according to their stacking errors. Model resolution matrices were calculated for the surface and tree inversions. The model resolution matrix describes the relation between the model parameters and the estimates such that

$$\mathbf{R} = \left[\mathbf{J}^T W_D^T W_D \mathbf{J} + \beta W_m^T \boldsymbol{W_m}\right]^{-1} \mathbf{J}^T W_D^T W_D \mathbf{J} \qquad (2)$$

where $\mathbf{J}$ is the Jacobian matrix from the inversion. For non-linear problems, $\mathbf{R}$ can be estimated using the $\mathbf{J}$ and β from the last iteration of the inversion (e.g., Alumbaugh and Newman, 2000).

A finite-element mesh was created with 5 cm × 5 cm elements to 60 cm depth and 350 cm width. Outside this area, element size gradually increased, totaling 2400 elements. A half space was used for the inversion. While there is some variability in the electrode placement in the field from the ideal map shown in Fig. 2a, the microtopographic variations are much smaller than the maximum pseudodepth of the acquisition; consequently, these effects were considered minimal with respect to the inversion.

Temperature corrections were performed on the inversions within the soil and the tree xylem to eliminate the effects of vary-ing temperatures over the daily (e.g., Fig. 4a) and monthly periods according to:

$$\sigma(T) = \sigma(T_0)[1 + \alpha(T - T_0)] \qquad (3)$$

where σ is apparent conductivity (Ω m), T is in situ temperature (°C), T_0 is the reference temperature (10 °C in this case), α is the fractional change in conductivity per change in degree Celsius and equal to 0.02 (Campbell et al., 1948). Temperature data from the eight temperature probes at varying locations and depths were compiled into a matrix and linearly interpolated between data collection points.

2.5. Tree survey inversions

Tree survey inversion of apparent electrical conductivities were performed with a code developed in Comsol Multiphysics that was modified to fit a 2.5D model in a circular domain using the same objective function as described by Eq. (1). To fit the shape of the tree trunk, a triangular mesh was used for both forward and inverse modeling. There were 616 triangular elements used for inversion and each of the inversion elements was further divided into four smaller triangular elements during forward modeling for convergence purposes. Compared with inversion for surface survey above, it is not obvious to define a derivative on the triangular mesh used for the tree, so the weighting matrix $\boldsymbol{W_m}$ was defined according to Binley et al. (1996), where the connection among all the triangular elements was decided and adjacent triangles for each triangle in the model domain were counted. If one triangle was surrounded by three other triangles, assigning a value of −3 on the diagonal elements $\boldsymbol{W_m}$ was assigned and 1 for the three adjacent triangles on each row.

The 2.5D model was validated by comparing forward model results of the circular domain to a slice of a 3D cylinder model inversion where the ERI survey was collected in the center (half-length) of the cylinder. An insulation boundary was assigned everywhere for the 3D model. For the validation, we used a homogenous mean value 500 Ωm (2 mS/m) for the resistivity, which was close to the mean value for our field data. When the height of the cylinder was at least 0.75 m (thus the ERI survey would need to be 0.375 m above the ground) the 2.5D and 3D models matched within 3% relative error. At lower heights the boundaries began to have significant influence. The ERI survey in the tree is approximately 1 m above ground so the 2.5D model gives a good approximation of the more realistic but computationally expensive 3D model.

3. Results and discussion

3.1. Data within the soil

The resulting tomograms depict a smoothed representation of the bulk electrical conductivity within the soil plot (Fig. 5c). The resolution of the inversion varied across the model space due to both data collection and the extent of smoothing within the model (Fig. 5b). The diagonal of the resolution matrix describes the degree to which the data informed the value of each pixel, and showed a mean range of percent differences from −7% to 3% and −8% to 10% from one inversion to the next over a 24-h period and a 6-month period, respectively, and were considered small for the work presented here. Spatially, the resolution of the inversion decreases with depth and was lowest toward the bottom corners of the reconstructed maps (Fig. 5b).

While the non-time-lapse inversions vary reasonably smoothly and have low variability (Fig. 5d), the spatial distribution of the change in ground electrical conductivity was highly heterogeneous (Fig. 5c), and likely reflects heterogeneity in soil (hydric) properties
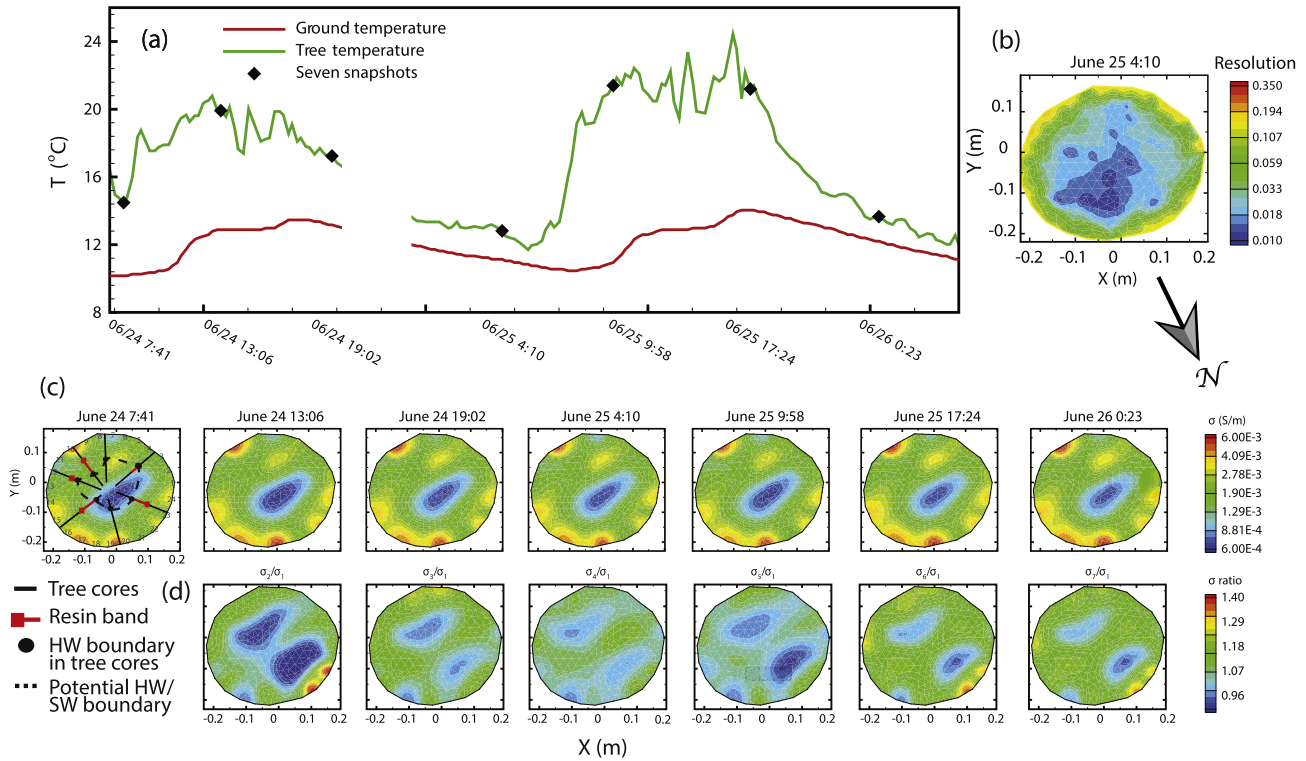
Fig. 4. Mean temperature from 10 to 20 cm depth from June 24 to 26, during which tree inversions were conducted (a). Representative resolution matrix of tree inversions (b). Resolution is highest toward the outside of the cross-section, where most changes are expected to occur. Electrical conductivity distribution of the tree through time in the top row (c), as well as differences from the first data set in the bottom row with respect to the data set from June 24 at 7:40 (d). Tree cores were collected at seven locations around the tree (c) and resin bands were found (squares). The depth to heartwood was measured from these cores and a potential heartwood/sapwood (HW/SW) boundary is shown by the dotted line.
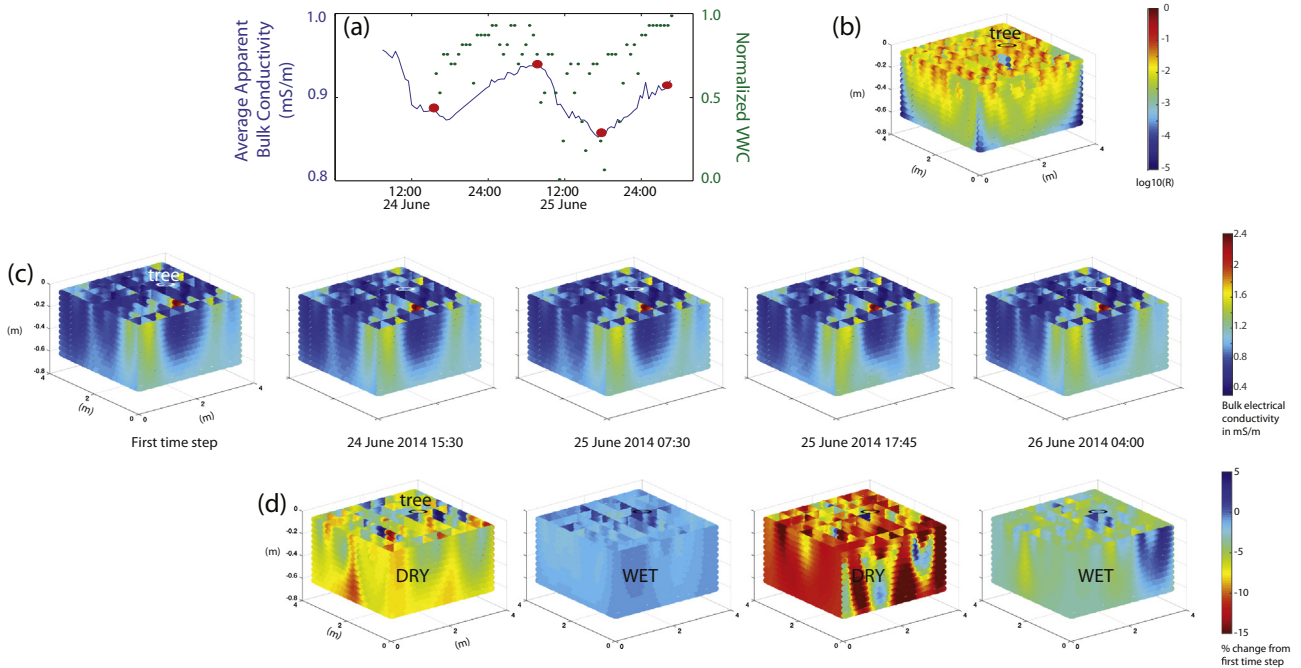
Fig. 5. Average apparent bulk electrical conductivity and volumetric water content at 10 cm (normalized to the maximum change) for a 48-h period from June 24 to June 26 (a), resolution map from the background data set as stitched 2-D line (b), and standard inversions (c) with time-lapse inversions of the same time steps below from four time steps differenced from June 24 at 7:40 where positive percent changes in conductivity indicate more wet soils (d). Images are stitched 2-D inversions. Higher percent change represents a decrease in soil moisture content. During the day the water content close to the tree is higher than the surrounding soil plot; in the early morning, the soil moisture content is higher throughout the site and shows less spatial variability. Z-axis scale is exaggerated on all stitched plots.

and in water uptake by roots. Similar variability has been seen in other research (e.g., Cassiani et al., 2015), including some work that was able to include destructive sampling (e.g., Amato et al., 2008). In general, the highest change in conductivity (regardless of time of day) was located closest to the tree (<0.5 m lateral distance), and decreased away from the tree until approximately 2.5 m, where it began to increase again (Fig. 5d). When the soil was very dry (Fig. 5d) there were some areas of higher change in conductivity that do not follow the radial pattern. The spatial distribution of the change in bulk electrical conductivity also varied with depth (Fig. 6). During the day, changes in conductivity were more spatially heterogeneous. In general, the change in conductivity was high near the tree at shallow depths, but low near the tree at deeper depths (Fig. 6). This result is likely a function of variation in the resolution of the inversion rather than hydrologic change within the system (Fig. 5b).

As the summer progressed, the average ground apparent conductivity generally decreased from 1.3 mS/m to 0.65 mS/m due to the seasonal drying of the soil (Fig. 7). Ground apparent conductivity temporarily increased from a daily mean of 0.79 mS/m on July 16 to 0.92 mS/m on August 4 and returned to 0.72 mS/m on September 3 (Fig. 7) associated with the summer monsoon season that caused a temporary increase in soil moisture. The magnitude of daily fluctuations of ground apparent conductivity showed a decreasing trend from early spring to late summer (Fig. 8), which was likely caused by the combined effects of declining soil moisture and a shift in source water for transpiration from shallow soil water to deeper water sources below the depth of investigation of the ERI data. We note that the moisture content data in Fig. 7 are from a nearby site because our data onsite were not continuous. While these additional data provide a continuous record, these sensors were not close enough to tree roots to show the diel signal present at our site and shown in Fig. 5a. Additionally, our moisture content data, collected using EC5s, have not been temperature corrected; however, moisture contents measured via these probes are related to temperature variations (Bogena et al., 2007; Rosenbaum et al., 2011). The variation in soil temperature is approximately 2 °C over a given day at 10 cm depth, which leads to a difference in estimated moisture content of 0.2%. While the absolute values on these moisture content probes were incorrect, the difference in moisture content was on the order of 1%.

3.2. ERI variations in the ponderosa pine trunk

As previously mentioned, 40% of the survey data could not be used for the inversion due to the high contact resistance from some of the electrodes. The locations of the available data varied among those surveys, so we selected a consistent 108 measurements for each time step that were used to minimize resolution variation between data sets. A resolution analysis was performed on the inversions to evaluate the resolution distribution with these available measurements; one example is plotted for one time step during the June 24–June 26 data collection period (Fig. 4b). In this time step and all others, the resolution is high close to the boundary and decreases toward the center of the tree trunk. This distribution is expected, as the electrodes are located just inside the surface of the bark. Results within the outer regions of the tree trunk can be regarded with confidence, while the results within the inner regions are less robust due to lower resolution.

ERI data on the tree bole cross-section revealed a spatially heterogeneous distribution of conductivity that varies in time (Fig. 4c). The inner bole conductivity values ranged from 5 to 10 times lower than the outer area, similar to previous ERI studies (e.g., Martin, 2012; Guyot et al., 2013), although we note that variations in resolution should be considered when exploring these data beyond anything qualitative. Using the seven tree cores collected around the circumference of the tree, we explored whether heartwood formation could explain areas of low conductivity within the inner bole. There were resinous portions in 5 of the 7 cores, which were likely evidence of the wood transitioning from sapwood to heartwood (Fig. 4c). This diffuse transition wood creates irregularities in conductivity, making the ERI delineation of the heartwood boundary difficult, especially when considering the low resolution in this inner core region. However, we were primarily interested in changes within the sapwood, putting higher priority on data in the outer xylem. We found variability in conductivity throughout the tree bole to be likely primarily linked to variations in wood water content; wood cores showed that gravimetric water content (based on wet weight) for the sapwood was 0.49 versus 0.29 for the heartwood.

The distribution of the higher conductivity (sapwood) areas was not uniform around the tree, with patches of high conductivity on the south and north to east sides of the cross-section and slightly lower conductivity patches on the northwest side (Fig. 4c). The patches were present despite the time of day (Fig. 4c), but the conductivity of these patches varied during the diel cycle with higher changes in conductivity during peak sap flow periods (Fig. 4d). While asymmetry was expected due to predominant wind and sunlight directions, the locations of some of the asymmetry seen in the study tree were not expected. Typically, there is more sap flow activity on the sunlit side of the tree (Hagrey, 2006), so higher conductivity was expected to be located on the south side of the tree. The patch with the highest consistent conductivity values is located on the south side of the tree, between electrodes 8 and 10. However, a second high conductivity anomaly is located on the NE side of the outer portion of the tree between electrodes 14 and 20 (Fig. 4c).
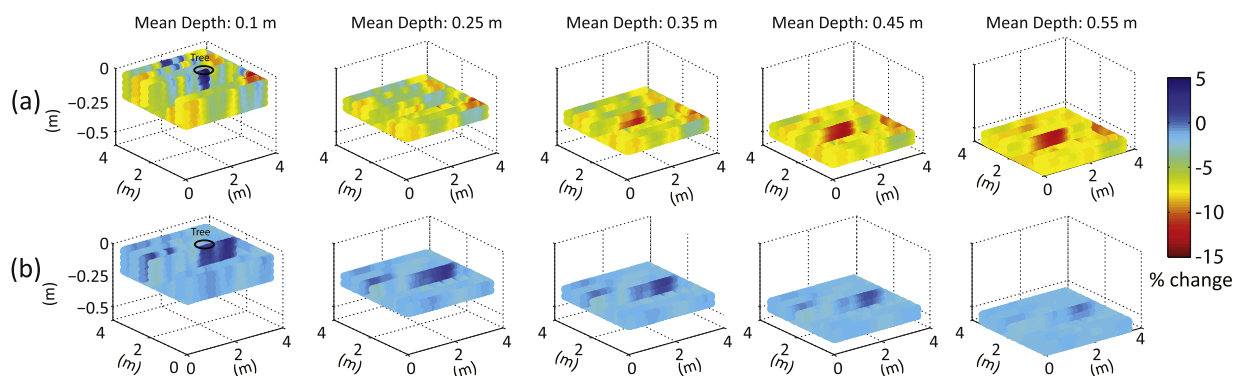

Fig. 6. Resistivity percent change for two times during the June 24–June 26 data collection period at different depths: June 24 at 15:26 (a) and June 25 at 07:25 (b). Difference inversions are with respect to June 24 at 7:40.
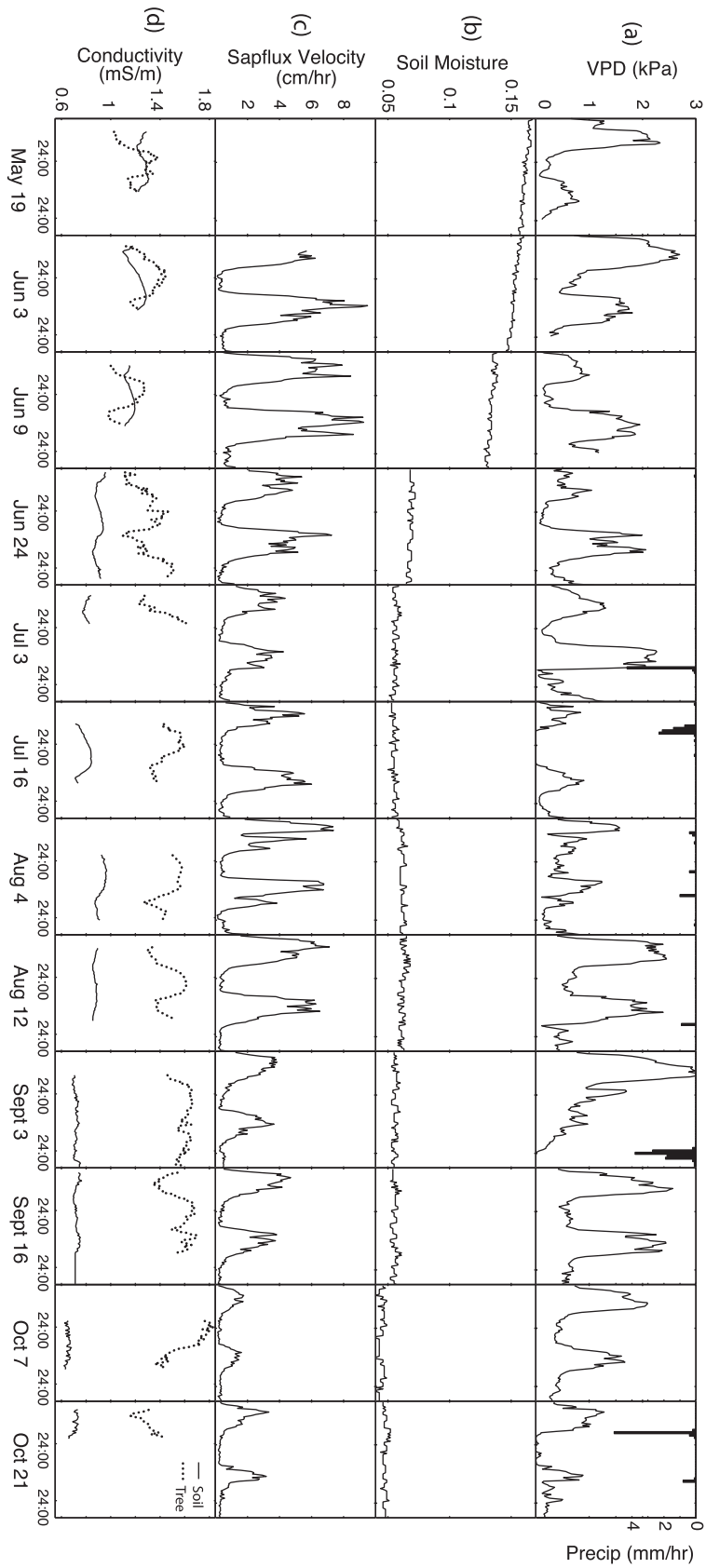
Fig. 7. Vapor pressure deficit (VPD) and precipitation during each collection period (a), average volumetric water content from the neighboring site (b), average sap flux velocity in the seven instrumented trees (c), average apparent tree conductivity in the study tree (dotted lines in d), and average apparent ground conductivity on the plot (solid lines in d). Note that the water content data shown here were collected off site and thus do not show the diel cycling seen on our site.
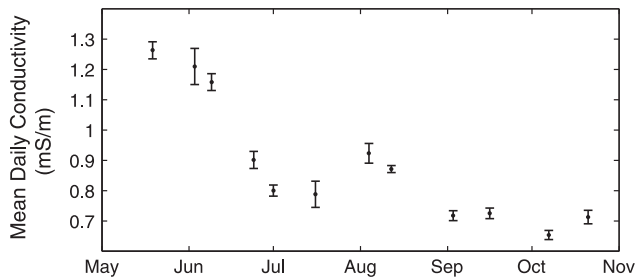
Fig. 8. Daily mean apparent conductivity (mS/m) in the subsurface for each data collection period decreased from late spring (May) to late fall (October). Error bars are the standard deviation from the mean value of the ground conductivity over each two-day data collection period, giving an indication of the amplitude of the diel cycling for the collected data sets.

Temperature can have a large effect on electrical conductivity. While bole temperature data were collected at three points around the tree, these data only correspond to the outer xylem, as temperature probes were inserted only 2 cm into the trunk. We expect that this outer xylem is exposed to the largest daily temperature changes (approximately 8 °C), and that the inner portion of the tree (the heartwood) likely does not experience as much temperature variation. However, we were unable to insert temperature probes deeply without damaging the tree. Little is known about thermal diffusion through tree trunks (e.g., Burgess et al., 2001; Vandegehuchte and Steppe, 2012), so it was not possible to confidently correct the data for temperature effects; however, during high transpiration times there was a notable decrease in bulk electrical conductivity within the tree (Fig. 7c and d).

While bulk conductivity increased with transpiration in portions of the sapwood, the average conductivity of the entire bole cross-section showed a different pattern. During low periods of sap flow (<50% of daily mean) within a given diel cycle, bulk tree conductivity was high (Fig. 7c and d). As sap flow increased during the day, the bulk conductivity within the tree decreased. We propose that this daily cycle is due to the refilling of water storage within the tree. In arid and semi-arid climates, soil-water availability becomes low in the dry summer months, thus increasing the vulnerability to embolism (air within the xylem), especially in tall trees where the tension within the xylem is higher. Ponderosa pines have been found to minimize this vulnerability by avoiding detrimental levels of xylem tension via use of stored water and radial movement of water between xylem conduits (Barnard et al., 2011). Phillips et al. (2003) found that use of stored water was concentrated to favorable times for photosynthesis, typically in the morning and early afternoon. Thus, the lower conductivity values within the tree during the day are likely due to lower bulk water content within the tree as it uses stored water. When sap flow decreases in the late afternoon, the bulk conductivity increases as the tree refills the stored water.

Over the growing period from May to the beginning of October, the average tree conductivity increased by 33%. Volumetric water content and nutrient uptake of ponderosa pines have been found to decrease during drier summer months (Domec et al., 2005), so this increase in conductivity is likely not due to changes in water content or nutrient concentrations. While the daily pattern in conductivity can be explained by tree water storage, as discussed above, the physical cause of the increasing seasonal pattern of bulk conductivity in the bole of the tree is not well understood.

3.3. Feedbacks between the tree and the subsurface

Diel patterns of ground apparent conductivity were related to diel sap flow patterns (Fig. 7c and d). From May to July, during the day when sapflow was high, apparent conductivity of the soil plot decreased by an average of 9% over the course of the day. During the night when sap flow reaches its minimum, the apparent conductivity of the soil increased by an average of 11% over the course of the night. We examined the correlations between average sapflow and ground apparent conductivity at 30-min time intervals for the dataset from June 24 to 26. The Pearson's correlation coefficient between sapflow and soil apparent conductivity was calculated for each 30-min lag (relating conductivity to sapflow at progressively earlier time periods) from 0 to 12 h. The strongest negative correlation was between soil apparent conductivity and sapflow is at about a 4 h lag; conductivity peaks 4 h after sapflow reaches it minimum. We believe that this lag is a function of the time it takes to refill the subsurface storage utilized by the tree. During transpiration, the water potential gradients from the soil to the root exceed those within the soil matrix, which causes water to flow into the tree, thus decreasing the soil moisture content of the plot. When transpiration ceases and the tree closes the stomata, the gradient between the root and soil decreases. This slows, and in some cases reverses, the depletion of soil moisture allowing for the soil within the rooting zone to be re-wetted.

While there is likely a difference in matric potential between the soil in the rooting zone of the tree and the surrounding soil, the gradient required to cause lateral movement of soil water would need to be relatively high in soil with such low moisture content. In a study that quantified hydraulic redistribution by *Artemisia tridentata*, Richards and Caldwell (1987) determined the amount of water replenished during a single night. Using combined diffusivity of the vapor and liquid phase in the soil, they determined it would take 2500–5000 days to transport the amount of nightly replenished water if soil water movement was the sole mechanism. Similarly, Domec et al. (2010) found that the capillary rise was <5% of the measured water that was being replenished overnight during the growing season. Soil water replenishment via soil alone is likely very small and slow in the semi-arid ecosystem our study, and not a primary mechanism for nocturnal soil moisture replenishment. Monitoring of the matric potential was not conducted in this study, but these measurements could be useful to further investigate spatiotemporal changes in matric potential gradients due to transpiration.

Because diffusion cannot explain increases in nocturnal soil moisture, we hypothesize that our diurnal variation in soil conductivity reflects a diurnal change in water content that could be driven by transpiration and hydraulic redistribution. The time series of normalized soil moisture data (Fig. 5a) show a nocturnal increase of soil moisture instead of a steady value, a pattern characteristic of hydraulic redistribution. Occasionally, the nocturnal increase exceeded the previous day's soil water maximum. Studies have found up to 35% of transpired water is due to hydraulic redistribution in ponderosa pines (Brooks et al., 2002). In loblolly pine, hydraulic redistribution maintained soil moisture above 0.15 and increased transpiration by 30–50%. Hydraulic redistribution accounted for 15–25% of measured total site water depletion seasonally with a maximum of approximately 1 mm/d (Domec et al., 2010). In a review of data from 16 different ecosystems, Neumann and Cardon (2012) found hydraulic redistribution varies by nearly two orders of magnitude across ecosystem with ponderosa pine values ranging from 0.2 to 1.0 mm/d. Similarly, in old growth ponderosa pine and Douglas-fir stands during dry conditions, hydraulic redistribution has been found to contribute an average of 0.1–0.2 mm/d of water use (e.g., Brooks et al., 2002; Meinzer et al., 2004; Warren et al., 2005, 2007). These ERI images (Fig. 5d), while of low resolution, indicate that there may be a larger contribution of hydraulic redistribution in this drier climate than in previous studies; changes in millimeters per day might be difficult to image with this technique. The ERI images showed

decreases in conductivity with depth, indicative of increased drying from the background case (Fig. 6a), suggesting that water is likely moving from areas deeper than our imaging to shallower, imaged, depths, but further investigation is needed to support this hypothesis.

The magnitude of daily fluctuations of ground conductivity decreased by 52% from June to October (Fig. 8). Several explanations could account for this result. In isohydric species such as ponderosa pine, one would expect tree transpiration to decline in response to declining soil moisture and matric potentials. This would result in smaller conductivity fluctuations due to less water being taken from the soil during the diel cycle. Data from June 9–10 to 24–26 support this hypothesis: with decreases in soil moisture (55%), decreases in sap flow (23%) and decreases in ground conductivity fluctuations (52%) occurring over this time period. This would suggest a soil-moisture-limited system. However, this hypothesis does not hold true for the entire summer. Data from June 24–26 and August 12–13 have similar average daily soil moisture contents (0.07 and 0.06, respectively), average daily sap flow (3.4 cm/h and 3.8 cm/h, respectively), and average daily apparent ground conductivity (0.90 mS/m and 0.87 mS/m, respectively). However, the average daily fluctuation of ground conductivity is 58% higher for June 24–26 than August 12–13. This could be due to the tree drawing water from a deeper, perhaps more consistent water source during August when the tree has been subjected to drier antecedent conditions. This has been found to occur in ponderosa pine stands during very dry conditions in northeast Oregon (Warren et al., 2007), and Licata et al. (2008) found that in young ponderosa pine, 20–40% of total transpired water was taken up from soil depths below 1 m during dry periods.

3.4. Data limitations

We acknowledge that many uncertainties exist in these data. The main source of uncertainty in the acquisition of tree resistivity is the contact resistances, which are high. The main source of uncertainty in the interpretation is that variations of resistivity will be sensitive to two distinct effects: temperature and water content, and possibly salinity if the ionic strength of the sap is expected to change. There are also a few other factors that could affect our interpretations of connections between transpiration and soil moisture such as the effect of root biomass and changes in pore water conductivity through selective ion uptake by the roots. However, we believe that the area of influence of these factors is likely local, and primarily in the rhizosphere around the root; additionally, ion concentrations within the tree go down during the day, not up, or in some cases they stay constant (Ferguson et al., 1983; Herdel et al., 2001; Mengel et al., 2001; Peuke et al., 2001). It is also difficult to separate the impacts on soil moisture movement in the subsurface from neighboring trees, and we note that additional studies on multiple trees would allow a statistical analysis not available here.

4. Conclusions

We present the first time-lapse ERI dataset mapping changes in a connected tree–soil system. We found that the spatial distribution of decreases in soil moisture is not homogeneous; variability in soil moisture changes in both vertical and lateral directions is likely due to root distribution and preferential pathways toward the roots. We hypothesize that a combination of matric potential-driven water movement, which is likely small, and hydraulic redistribution drives diel re-wetting process of the soil and further investigations should include matric potential measurements to properly address the soil moisture pathways. Our

data suggest a switch of tree water source from the shallow soil profile early in the growing season to deeper water as drought conditions persist.

Although changes in transpiration rates were not explicitly determined from the ERI data, ERI did capture the timing of the daily conductivity change in the tree and the spatiotemporal variability of active sapwood. The results of the ERI surveys on the tree trunk show many of the common considerations in upscaling sap flow are appropriate (e.g. variation in sapflux rates between the inner and outer xylem), but are grossly overgeneralized and do not account for potential cross-sectional variability. To further explore how the subsurface water storage processes influence the connection between transpiration and streamflow, a combination of hillslope-scale geophysical and isotopic methods could be used.

Appendix A. Supplementary material

Supplementary data associated with this article can be found, in the online version, at http://dx.doi.org/10.1016/j.jhydrol.2016.03.003.

References

Alumbaugh, D.L., Newman, G.A., 2000. Image appraisal for 2-D and 3-D electromagnetic inversion. Geophysics 65, 1455–1467.
Amato, M., Basso, B., Celano, G., Bitella, G., Morelli, G., Rossi, R., 2008. In situ detection of tree root distribution and biomass by multi-electrode resistivity imaging. Tree Physiol. 28 (10), 1441–1448.
Banton, O., Seguin, M.K., Cimon, M.A., 1997. Mapping field-scale physical properties of soil with electrical resistivity. Soil Sci. Soc. Am. J. 61, 1010–1017.
Barnard, H.R., Graham, C.B., Van Verseveld, W.J., Brooks, J.R., Bond, B.J., McDonnell, J. J., 2010. Mechanistic assessment of hillslope transpiration controls of diel subsurface flow: a steady-state irrigation approach. Ecohydrology 3, 133–142. http://dx.doi.org/10.1002/eco.114.
Barnard, D.M., Meinzer, F.C., Lachenbruch, B., Mcculloh, K.A., Johnson, D.M., Woodruff, D.R., 2011. Climate-related trends in sapwood biophysical properties in two conifers: avoidance of hydraulic dysfunction through coordinated adjustments in xylem efficiency, safety and capacitance. Plant, Cell Environ. 34, 643–654.
Beff, L., Gunther, T., Vandoorne, B., Couvreur, V., Javaux, M., 2013. Three-dimensional monitoring of soil water content in a maize field using Electrical Resistivity Tomography. Hydrol. Earth Syst. Sci. 17, 595–609.
Befus, K.M., Sheehan, A.F., Leopold, M., Anderson, S.P., Anderson, R.S., 2011. Seismic constraints on critical zone architecture, Boulder Creek Watershed, Front Range, Colorado. Vadose Zone J. 10, 915.
Berndt, H.W., Gibbons, R.D., 1958. Root distribution of some native and understory plants growing on three sites within the ponderosa pine watershed in Colorado. Station Paper No. 37. USDA Forest Service, Rocky Mountain Forest and Range Experiment Station, Fort Collins, CO.
Bieker, D., Rust, S., 2010. Electric resistivity tomography shows radial variation of electrolytes in Quercus robur. Can. J. For. Res. 40.
Binley, A., Kemna, A., 2005. DC resistivity and induced polarization methods. In: Rubin, Y., Hubbard, S.S. (Eds.), Hydrogeophysics, pp. 129–156.
Binley, A.M., Henry-Poulter, S., Shaw, B., 1996. Examination of solute transport in an undisturbed soil column using electrical resistance tomography. Water Resour. Res. 32, 763–769.
Bleby, T.M., McElrone, A.J., Jackson, R.B., 2010. Water uptake and hydraulic redistribution across large woody root systems to 20 m depth. Plant, Cell Environ. 33, 2132–2148.

Bogena, H.R., Huisman, J.A., Oberdörster, C., Vereecken, H., 2007. Evaluation of a low-cost soil water content sensor for wireless network applications. J. Hydrol. 344 (1), 32–42.

Bond, B.J., Jones, J.A., Moore, G., Phillips, N., Post, D., McDonnell, J.J., 2002. The zone of vegetation influence on baseflow revealed by diel patterns of streamflow and vegetation water use in a headwater basin. Hydrol. Process. 16, 1671–1677.

Boronina, A., Golubev, S., Balderer, W., 2005. Estimation of actual evapotranspiration from an alluvial aquifer of the Kouris catchment (Cyprus) using continuous streamflow records. Hydrol. Process. 19, 4055–4068 (26).

Bouyoucos, G.J., Mick, A.H., 1940. An electrical resistance method for the continuous measurement of soil moisture under field conditions. Tech. Bull. Michigan Agric. Exp. Stn. No. 172.

Brooks, J.R., Meinzer, F.C., Coulombe, R., Gregg, J., 2002. Hydraulic redistribution of soil water during summer drought in two contrasting Pacific Northwest coniferous forests. Tree Physiol. 22, 1107–1117.

Brooks, R.J., Barnard, H.R., Coulombe, R., McDonnell, J.J., 2010. Ecohydrologic separation of water between trees and streams in a Mediterranean climate. Nat. Geosci., 100–104

Brunet, P., Clément, R., Bouvier, C., 2010. Monitoring soil water content and deficit using Electrical Resistivity Tomography (ERT) – a case study in the Cevennes area, France. J. Hydrol. 380, 146–153.

Burgess, S.S.O., Adams, M.A., Turner, N.C., Ong, C.K., 1998. The redistribution of soil water by tree root systems. Oecologia 115, 306–311.

Burgess, S.S., Adams, M.A., Turner, N.C., Beverly, C.R., Ong, C.K., Khan, A.A., Bleby, T. M., 2001. An improved heat pulse method to measure low and reverse rates of sap flow in woody plants. Tree Physiol. 21 (9), 589–598.

Burgess, S.S.O., Pate, J.S., Adams, M.A., Dawson, T.E., 2000. Seasonal water acquisition and redistribution in the Australian woody phreatophyte, Banksia prionotes. Ann. Bot., 215–224

Butler, J.J., Kluitenberg, G.J., Whittemore, D.O., Loheide, S.P., Jin, W., Billinger, M.A., Zhan, X., 2007. A field investigation of phreatophyte-induced fluctuations in the water table. Water Resour. Res. 43, W02404. http://dx.doi.org/10.1029/2005WR004627.

Caldwell, M.M., Richards, J.H., 1989. Hydraulic lift: water efflux from upper roots improves effectiveness of water uptake by roots. Oecologia 79, 1–5.

Campbell, R.B., Bower, C.A., Richards, L.A., 1948. Change of electrical conductivity with temperature and the relation of osmotic pressure to electrical conductivity and ion concentration for soil extracts. Soil Sci. Soc. Proc., 66–69

Cassiani, G., Boaga, J., Vanella, D., Perri, M.T., Consoli, S., 2015. Monitoring and modelling of soil–plant interactions: the joint use of ERT, sap flow and Eddy Covariance data to characterize the volume of an orange tree root zone. Hydrol. Earth Syst. Sci. 19 (5), 2213–2225.

Chambers, J.E., Gunn, D., Wilkinson, P.B., Meldrum, P.I., Haslam, E., Holyoake, S., Kirkham, M., Kuras, O., Merritt, A., Wragg, J., 2014. 4D electrical resistivity tomography monitoring of soil moisture dynamics in an operational railway embankment. Near Surf. Geophys. 12, 61–72.

Daily, W., Ramirez, A., LaBrecque, D., Nitao, J., 1992. Electrical resistivity tomography of vadose water movement. Water Resour. Res. 28 (5), 1429–1442. http://dx.doi.org/10.1029/91WR03087.

Dawson, T.E., 1993. Hydraulic lift and water use by plants: implications for water balance, performance and plant–plant interactions. Oecologia 95, 565–574.

Dawson, T.E., Ehleringer, J.R., 1991. Streamside trees that do not use stream water. Nature 350, 335–337.

Day-Lewis, F.D., Singha, K., Binley, A., 2005. The application of petrophysical models to radar and electrical resistivity tomograms: resolution-dependent limitations. J. Geophys. Res. 110, B08206. http://dx.doi.org/10.1029/2004JB003569 (17 p.).

Dey, A., Morrison, H.F., 1979. Resistivity modelling for arbitrarily shaped two-dimensional structures. Geophys. Prospect. 27 (1), 106–136.

Dobriyal, P., Qureshi, A., Badola, R., Hussain, S.A., 2012. A review of the methods available for estimating soil moisture and its implications for water resource management. J. Hydrol. 458, 110–117. http://dx.doi.org/10.1016/j.jhydrol.2012.06.021.

Domec, J., Pruyn, M.L., Gartner, B.L., 2005. Axial and radial profiles in conductivities, water storage and native embolism in trunks of young and old-growth ponderosa pine trees. Plant, Cell Environ. 28, 1103–1113.

Domec, J., King, J.S., Noormets, A., Treasure, E., Gavazzi, M.J., Sun, G., Mcnulty, S.G., 2010. Hydraulic redistribution of soil water by roots affects whole-stand evapotranspiration and net ecosystem carbon exchange. New Phytol., 171–183

Evaristo, J., Jasechko, S., McDonnell, J.J., 2015. Global separation of plant transpiration from groundwater and streamflow. Nature 525 (7567), 91–94.

Fan, J., Scheuermann, A., Guyot, A., Baumgartl, T., Lockington, D.A., 2015. Quantifying spatiotemporal dynamics of root-zone soil water in a mixed forest on subtropical coastal sand dune using surface ERT and spatial TDR. J. Hydrol. 523, 475–488.

Fiora, A., Cescatti, A., 2006. Diurnal and seasonal variability in radial distribution of sap flux density: implications for estimating stand transpiration. Tree Physiol. 26, 1217–1225.

Ford, C.R., Guire, M.A.M.C., Mitchell, R.J., Teskey, O., 2004. Assessing variation in the radial profile of sap flux density in Pinus species and its effect on daily water use. Tree Physiol. 24, 241–249.

Friedman, S.P., 2005. Soil properties influencing apparent electrical conductivity: a review. Comput. Electron. Agric. 46 (1), 45–70.

Ferguson, A.R., Eiseman, J.A., Leonard, J.A., 1983. Xylem sap from Actinidia chinensis: seasonal changes in composition. Ann. Bot. 51 (6), 823–833.

Garré, S., Javaux, M., Vanderborght, J., Vereecken, H., 2011. Three-dimensional electrical resistivity tomography to monitor root zone water dynamics. Vadose Zone J. 10 (1), 412–424.

Garré, S., Coteur, I., Wongleecharoen, C., Kongkaew, T., Diels, J., Vanderborght, J., 2013. Noninvasive monitoring of soil water dynamics in mixed cropping systems: a case study in Ratchaburi Province, Thailand. Vadose Zone J. 12 (2).

Ghannam, K., Nakai, T., Paschalis, A., Oishi, C.A., Kotani, A., Igarashi, Y., Kumagai, T., Katul, G.G., 2016. Persistence and memory timescales in root-zone soil moisture dynamics. Water Resour. Res. 52. http://dx.doi.org/10.1002/2015WR017983.

Gibert, D., Le Mouël, J.L., Lambs, L., Nicollin, F., Perrier, F., 2006. Sap flow and daily electric potential variations in a tree trunk. Plant Sci. 171 (5), 572–584.

Good, S.P., Noone, D., Bowen, G., 2015. Hydrologic connectivity constrains partitioning of global terrestrial water fluxes. Science 349 (6244), 175–177.

Gora, E.M., Yanoviak, S.P., 2015. Electrical properties of temperate forest trees: a review and quantitative comparison with vines. Can. J. For. Res. 45, 236–245.

Graham, C.B., Barnard, H.R., Kavanaugh, K., McNamara, J., 2013. Catchment scale controls temporal connection of transpiration and diel fluctuations in streamflow. Hydrol. Process. http://dx.doi.org/10.1002/hyp.9334.

Granier, A., 1987. Evaluation of transpiration in a Douglas-fir stand by means of sap flow measurements. Tree Physiol. 3, 309–320.

Guyot, A., Ostergaard, K.T., Lenkopane, M., Fan, J., Lockington, D., 2013. Using electrical resistivity tomography to differentiate sapwood from heartwood: application to conifers. Tree Physiol. 33, 187–194.

Hagrey, S.A., 2006. Electrical resistivity imaging of tree trunks. Near Surf. Geophys. 4, 179–187.

Hagrey, S.A., Michaelsen, J., 2002. Hydrogeophysical soil study at a drip irrigated orchard, Portugal. Eur. J. Environ. Eng. Geophys. 7, 75–93.

Herdel, K., Schmidt, P., Feil, R., Mohr, A., Schurr, U., 2001. Dynamics of concentrations and nutrient fluxes in the xylem of Ricinus communis – diurnal course, impact of nutrient availability and nutrient uptake. Plant, Cell Environ. 24 (1), 41–52.

Hewlett, J.D., 1982. Principles of Forest Hydrology. University of Georgia Press, 192pp.

Hinckley, E.S., Ebel, B.A., Barnes, R.T., Anderson, R.S., Williams, M.W., Anderson, S.P., 2014. Aspect control of water movement on hillslopes near the rain–snow transition of the Colorado Front Range. Hydrol. Process. 28. http://dx.doi.org/10.1002/hyp.9549.

Hussain, K., Wongleecharoen, C., Hilger, T., Vanderborght, J., Garré, S., Onsamrarn, W., Sparke, M.-A., Diels, J., Kongkaew, T., Cadisch, G., 2015. Combining $\delta^{13}C$ measurements and ERT imaging: improving our understanding of competition at the crop-soil-hedge interface. Plant Soil, 1–20.

Jayawickreme, D.H., Van Dam, R.L., Hyndman, D.W., 2010. Hydrological consequences of land-cover change: quantifying the influence of plants on soil moisture with time-lapse electrical resistivity. Geophysics 75 (4), WA43–WA50.

Licata, J.A., Gyenge, J.E., Fernández, M.E., Schlichter, T.M., Bond, B.J., 2008. Increased water use by ponderosa pine plantations in northwestern Patagonia, Argentina compared with native forest vegetation. For. Ecol. Manage. 255 (3), 753–764.

Maeght, J.-L., Rewald, B., Pierret, A., 2013. How to study deep roots-and why it matters. Front. Plant Sci. 4, 299.

Martin, T., 2012. Complex resistivity measurements on oak. Eur. J. Wood Wood Prod. 70, 45–53.

Meinzer, F.C., Brooks, J.R., Bucci, S., Goldstein, G., Scholz, F.G., 2004. Converging patterns of uptake and hydraulic redistribution of soil water in contrasting woody vegetation types. Tree Physiol., 919–928

Mengel, K., Kosegarten, H., Kirkby, E.A., Appel, T. (Eds.), 2001. Principles of Plant Nutrition. Springer Science & Business Media.

Michot, D., Benderitter, Y., Dorigny, A., Nicoullaud, B., King, D., Tabbagh, A., 2003. Spatial and temporal monitoring of soil water content with an irrigated corn crop cover using surface electrical resistivity tomography. Water Resour. Res. 39, 1–20.

Monteith, J.L., Unsworth, M.H., 1990. Principles of Environmental Physics. Edward Arnold, London, 290pp.

Moore, G.W., Jones, J.A., Bond, B.J., 2011. How soil moisture mediates the influence of transpiration on streamflow at hourly to interannual scales in a forested catchment. Hydrol. Process. 25, 3701–3710. http://dx.doi.org/10.1002/hyp.8095.

Natural Resources Conservation Service Soil Survey, United States Department of Agriculture. Web Soil Survey. <http://websoilsurvey.nrcs.usda.gov/> (accessed April 20 2015).

Neumann, R.B., Cardon, Z.G., 2012. Tansley review: the magnitude of hydraulic redistribution by plant roots: a review and synthesis of empirical and modeling studies. New Phytol., 337–352

Nicolotti, G., Socco, L.V., Martinis, R., Godio, A., Sambuelli, L., 2003. Application and comparison of three tomographic techniques for detection of decay in trees. J. Arboric. 29, 66–78.

Nijland, W., van der Meijde, M., Addink, E.A., de Jong, S.M., 2010. Detection of soil moisture and vegetation water abstraction in a Mediterranean natural area using electrical resistivity tomography. Catena 81, 209–216.

Peuke, A.D., Rokitta, M., Zimmermann, U., Schreiber, L., Haase, A., 2001. Simultaneous measurement of water flow velocity and solute transport in xylem and phloem of adult plants of Ricinus communis over a daily time course by nuclear magnetic resonance spectrometry. Plant, Cell Environ. 24 (5), 491–503.

R. Mares et al./Journal of Hydrology 536 (2016) 327–338

Phillips, N.G., Ryan, M.G., Bond, B.J., McDowell, N.G., Hinckley, T.M., Cermák, J.È., 2003. Reliance on stored water increases with tree size in three species in the Pacific Northwest. Tree Physiol. 23, 237–245.

Reigner, I.C., 1966. A method of estimating streamflow loss by evapotranspiration from the riparian zone. For. Sci. 12, 130–139.

Richards, J.H., Caldwell, M.M., 1987. Hydraulic lift: substantial nocturnal water transport between soil layers by *Artemisia tridentata* roots. Oecologia 73, 486–489.

Rosenbaum, U., Huisman, J.A., Vrba, J., Vereecken, H., Bogena, H.R., 2011. Correction of temperature and electrical conductivity effects on dielectric permittivity measurements with ECH_2O sensors. Vadose Zone J. 10 (2), 582–593.

Ryan, M.G., Bond, B.J., Law, B.E., Hubbard, R.M., Woodruff, D., Cienciala, E., Kucera, J., 2000. Transpiration and whole-tree conductance in ponderosa pine trees of different heights. Oecologia 124 (4), 553–560.

Samouëlian, A., Cousin, I., Tabbagh, A., Bruand, A., Richard, G., 2005. Electrical resistivity survey in soil science: a review. Soil Tillage Res. 83 (2), 173–193.

Schwartz, B.F., Schreiber, M.E., Yan, T., 2008. Quantifying field-scale soil moisture using electrical resistivity imaging. J. Hydrol. 362, 234–246.

Schenk, H.J., Jackson, R.B., 2002. Rooting depths, lateral root spreads and below-ground/above-ground allometries of plants in water-limited ecosystems. J. Ecol. 90 (3), 480–494.

Skutt, H.R., Shigo, A.L., Lessard, R.A., 1972. Detection of discolored and decayed wood in living trees using a pulsed electric current. Can. J. For. Res. 2, 54–56.

Srayeddin, I., Doussan, C., 2009. Estimation of the spatial variability of root water uptake of maize and sorghum at the field scale by electrical resistivity tomography. Plant Soil 319 (1–2), 185–207.

Steppe, K., De Pauw, D.J., Doody, T.M., Teskey, R.O., 2010. A comparison of sap flux density using thermal dissipation, heat pulse velocity and heat field deformation methods. Agric. For. Meteorol. 150 (7), 1046–1056.

Stone, E.L., Kalisz, P.J., 1991. On the maximum extent of tree roots. For. Ecol. Manage. 46 (1), 59–102.

Tattar, T., Shigo, A., Chase, T., 1972. Relationship between the degree of resistance to a pulsed electric current and wood in progressive stages of discoloration and decay in living trees. Can. J. For. Res. 2 (3), 236–243.

Vandegehuchte, M.W., Steppe, K., 2012. Improving sap flux density measurements by correctly determining thermal diffusivity, differentiating between bound and unbound water. Tree Physiol. 32 (7), 930–942.

Vertessy, R.A., Hatton, T.J., Reece, P., Sullivan, S.K.O., Benyon, R.G., 1997. Estimating stand water use of large mountain ash trees and validation of the sap flow measurement technique. Tree Physiol. 17, 747–756.

Wang, H., Guan, H., Guyot, A., Simmons, C.T., Lockington, D.A., 2015. Quantifying sapwood width for three Australian native species using electrical resistivity tomography. Ecohydrology. http://dx.doi.org/10.1002/eco.1612.

Warren, J.M., Meinzer, F.C., Brooks, J.R., Domec, J.C., 2005. Vertical stratification of soil water storage and release dynamics in Pacific Northwest coniferous forests. Agric. For. Meteorol. 130, 39–58.

Warren, J.M., Meinzer, F.C., Brooks, J.R., Domec, J., Coulombe, R., Warren, J.M., 2007. Hydraulic redistribution of soil water in two old-growth coniferous forests: quantifying patterns and controls. New Phytol., 753–765

Werban, U., Attia al Hagrey, S., Rabbel, W., 2008. Monitoring of root-zone water content in the laboratory by 2D geoelectrical tomography. J. Plant Nutr. Soil Sci. 171 (6), 927–935.

Zhou, Q.Y., Shimada, J., Sato, A., 2001. Three-dimensional spatial and temporal monitoring of soil water content using electrical resistivity tomography. Water Resour. Res. 37, 273–285.